International Journal of Architectural, Civil and Construction Sciences
ISSN: 2415-1734
Vol:11, No:6, 2017

Performance Assessment of the Gold Coast Desalination Plant Offshore Multiport Brine Diffuser during 'Hot Standby' Operation

M. J. Baum, B. Gibbes, A. Grinham, S. Albert, D. Gale, P. Fisher

***Abstract*—**Alongside the rapid expansion of Seawater Reverse Osmosis technologies there is a concurrent increase in the production of hypersaline brine by-products. To minimize environmental impact, these by-products are commonly disposed into open-coastal environments via submerged diffuser systems as inclined dense jet outfalls. Despite the widespread implementation of this process, diffuser designs are typically based on small-scale laboratory experiments under idealistic quiescent conditions. Studies concerning diffuser performance in the field are limited. A set of experiments were conducted to assess the near field characteristics of brine disposal at the Gold Coast Desalination Plant offshore multiport diffuser. The aim of the field experiments was to determine the trajectory and dilution characteristics of the plume under various discharge configurations with production ranging 66 – 100% of plant operative capacity. The field monitoring system employed an unprecedented static array of temperature and electrical conductivity sensors in a three-dimensional grid surrounding a single diffuser port. Complimenting these measurements, Acoustic Doppler Current Profilers were also deployed to record current variability over the depth of the water column and wave characteristics. Recorded data suggested the open-coastal environment was highly active over the experimental duration with ambient velocities ranging 0.0 – 0.5 $m \cdot s^{-1}$, with considerable variability over the depth of the water column observed. Variations in background electrical conductivity corresponding to salinity fluctuations of ± 1.7 $g \cdot kg^{-1}$ were also observed. Increases in salinity were detected during plant operation and appeared to be most pronounced 10 – 30 m from the diffuser, consistent with trajectory predictions described by existing literature. Plume trajectories and respective dilutions extrapolated from salinity data are compared with empirical scaling arguments. Discharge properties were found to adequately correlate with modelling projections. Temporal and spatial variation of background processes and their subsequent influence upon discharge outcomes are discussed with a view to incorporating the influence of waves and ambient currents in the design of brine outfalls into the future.

M. J. Baum is with the School of Civil Engineering at The University of Queensland, St. Lucia, QLD 4072 Australia (phone: +61-413-069-721; e-mail: m.baum@uq.edu.au).

B. Gibbes is with the School of Civil Engineering at the University of Queensland, St. Lucia, QLD 4072 Australia (phone: +61-733-659-151; e-mail: b.gibbes@uq.edu.au).

A. Grinham and S. Albert are with the School of Civil Engineering at the University of Queensland, St. Lucia, QLD 4072 Australia (phone: +61-733-654-295; e-mail: a.grinham@uq.edu.au, s.albert@uq.edu.au).

D. Gale was with the School of Civil Engineering at the University of Queensland, St. Lucia, QLD 4072 Australia. She is now with Seqwater, 117 Brisbane St, Ipswich, QLD 4035 Australia (phone: +61-730-355-739; e-mail: Deb.Gale@seqater.com.au).

P. Fisher was with the School of Civil Engineering at the University of Queensland, St. Lucia, QLD 4072 Australia. He is now with Telstra, Locked Bag 6511, Sydney, NSW 2001 Australia (phone: +61-431-826-896; e-mail: p.l.fisher@hotmail.com).

***Keywords*—**Brine disposal, desalination, field study, inclined dense jets, negatively buoyant discharge.

I. Introduction

DRAMATIC climatological patterns in recent years have resulted in the subsequent investment in crisis resilient water supply infrastructure including Seawater Reverse Osmosis (SWRO) technologies [1]. Hypersaline by-products arising from SWRO production are commonly disposed into shallow, open-coastal environments. Due to their physio-chemical properties, such brine effluents are typically denser than their receiving ambient water body and descend to the seafloor, presenting a risk to benthic biota [2]. Mitigating these effects, dense effluents are frequently discharged via submerged, multiport diffusers, which are designed to eject concentrate at high velocity and at some intermediate angle above horizontal (60° inclination adopted as the de facto standard from the works of [3]) in order to maximize mixing and dilution.

The behavior of dense jets is notoriously complex. Industrial applications widely adopt empirical scaling arguments (such as those presented by [4]) to predict jet trajectory and associated brine dilution. While this approach appears suitable for environments subject to minimal ambient hydrodynamic activity, the shallow open-coastal settings typical of these discharges may differ considerably from the quiescent conditions on which design approaches are based.

Detailed field measurements of brine outfalls are limited, particularly those that seek to examine three-dimensional flow characteristics. Specifically, the trajectory and extent of inclined dense outfalls at field scale have not yet been measured in detail. Further, an understanding of transient hydrodynamic properties (that are characteristic of shallow open-coastal environments) and their influence on discharge response is limited. To address this information gap, hypersaline discharges from a submerged multiport diffuser with an intermediately inclined port orientation were examined using a combination of flow, and Conductivity-Temperature (CT) measurements to determine terminal rise and brine sub-layer properties. These sensors were deployed in a moored sensor array. Comparisons of these field measurements with quiescent-based empirical formulations are also made.

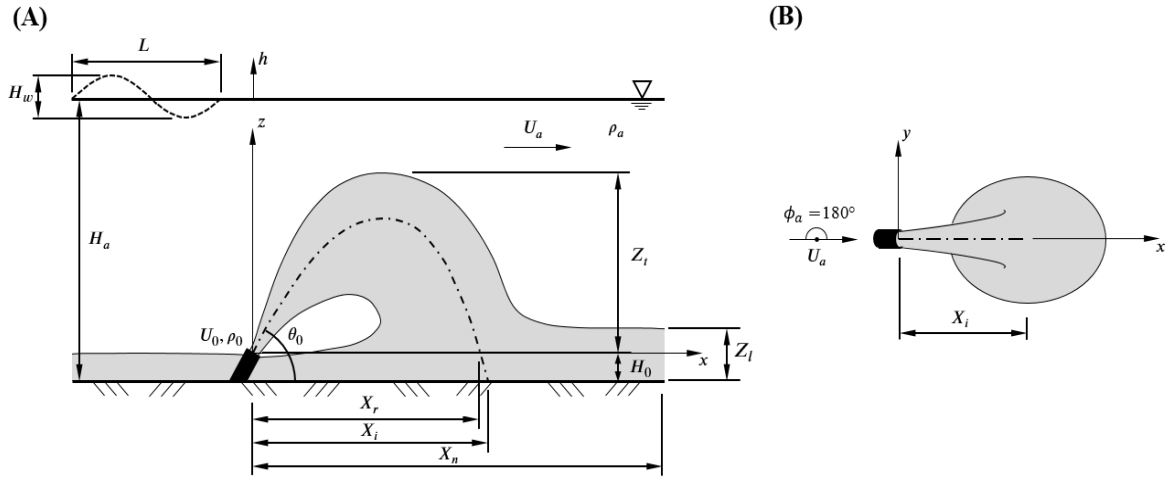

Fig. 1 Schematic of an inclined dense jet and nomenclature for key dimensional flow characteristics. (A) Side view. (B) Plan view

II. Analysis

The analysis of dense jet properties is well documented (e.g. [4], [5]–[7]). Semi-empirical length-scale evaluation of dense jet trajectory properties and their respective dilution properties has proven a useful approach to analyze these plumes. Parameters commonly used to describe the flows are presented in Fig. 1.

Effluent with density, ρ_0 [M L^{-3}], is discharged with velocity, U_0 [L T^{-1}], via a sharp-edged circular orifice with diameter, d [L], into a receiving water body with density, ρ_a [M L^{-3}]. The angle, θ_0 [-], is the inclination above the horizontal plane, where $\theta_0 = 60°$ is widely accepted as the de facto standard for these flows [4]. As the jet rises, flow is initially dictated by jet-momentum. However, due to the elevated density relative to the receiving ambient environment ($\rho_0 > \rho_a$), buoyancy forces prevail – causing the discharge to return to the lower boundary where it then spreads as a density current. Assuming flow is fully turbulent and the Boussinesq approximation is valid ($(\rho_0 - \rho_a) \ll \rho_a$), for a fixed discharge inclination angle, trajectory (χ) and dilution (S) parameters are given by [7]:

$$\frac{\chi}{dF}, \frac{S}{F} = f(u_r F, \phi_a) \quad (1)$$

where $F = U_0 / (g_0' d)^{1/2}$ [-] is the jet densimetric Froude number and $g_0' = g \times (\rho_0 - \rho_a) / \rho_a$ [L T^{-2}] is the modified acceleration due to gravity. The term u_r [-] relates the magnitude of ambient crossflow velocity (U_a [L T^{-1}]) to the jet velocity with the ratio $u_r = U_a / U_0$. The parameter $u_r F$ [-] is a type of crossflow Froude number. For $u_r F \ll 1$, the current has little effect on the jet, while for $u_r F \gg 1$ the jet is strongly dictated by ambient flow properties [8]. The parameter ϕ_a [-] is the angle of discharge propagation relative to ambient crossflow (Fig. 1 (B)). For a port inclined at $\theta_0 = 60°$, subjection to a counter-propagating current ($\phi_a = 0°$) with a crossflow magnitude of $u_r F \approx 0.67$ results in the discharge trajectory falling back on itself [8]. These characteristics form the basis of the analysis presented here.

III. Materials and Methods

A. Study Site Description

The Gold Coast Desalination Plant (GCDP) (-28.1578°, 153.4978°) multiport brine diffuser is situated ~1200 m offshore in an open coastal environment at an average depth of 17.7 m over a full spring-neap cycle. Brine concentrate is gravity-fed to the diffuser via a ~2300 m tunnel with a 2.8 m internal diameter, situated ~60 m deep [9]. The 203 m long diffuser consists of 14 diffuser ports oriented perpendicularly to the structure in an alternating configuration. Each port is inclined at 60° above the horizontal plane with a discharge elevation of 2.5 m above the seafloor. The diffuser is oriented perpendicularly to the coastline in an attempt to maximize mixing by longshore currents. The seafloor at the site is characterized by a relatively even sand substrate with a 1:68 gradient sloping near-parallel to the structure, heading offshore.

B. Field Experiment

Three operational regimes were considered in this study; 100% capacity, 66% capacity with diluted brine, and 66% capacity with minimal dilution. Given the wide spacing of the diffuser ports, discharges from the GCDP were expected to exhibit point source discharge behavior – analogous to singular port outfalls [10]. Based on this assumption, a static monitoring system was designed with the aim of resolving the spatial extent and behavior of a single discharge jet in near and intermediate field. The internal diameter, d, of the nominal port is 0.238 m. The field monitoring system consisted of a distributed network of sensors to assess water quality and hydrodynamic behavior. Deployed instrument locations are presented in Fig. 2.

The water quality monitoring system consisted of 25 sub-surface moorings deployed within approximately 60 m downstream of a nominal diffuser port. At 2.5 m elevation off the seabed, each sub-surface mooring was equipped with a

self-logging CT probe (Dataflow Systems, Christchurch, New Zealand). Each CT instrument was programmed to record with a 2-minute sampling frequency from 10 October 2013 to 3 November 2013.

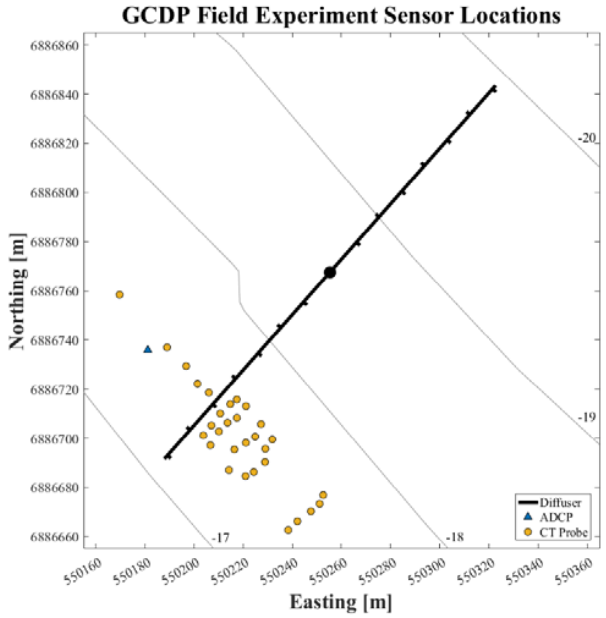

Fig. 2 GCDP diffuser, coastal bathymetry and relevant instrument deployment locations (± 5 m). Vertical depth contours are in meters AHD. Coordinated system is GDA 1994 MGA, Zone 56

A bottom-mounted, upward facing Acoustic Doppler Current Profiler (ADCP) instrument (1200 kHz Workhorse Sentinel with waves monitoring, Teledyne RDI, California, U.S.A) was deployed approximately 35 m upstream of the diffuser port that was the focus of the static monitoring system, from 6 October 2013 until 7 November 2013. The ADCP transducer elevation was recorded at 0.65 m above the seabed and had a blanking distance of 0.70 m. Velocity profile data was recorded for 20-minute averaging ensembles with a vertical bin resolution of 0.25 m. Wave height, period and direction were each sampled over 60-minute averaging ensembles. Direction measurements account for magnetic declination and are presented relative to true azimuths [11].

IV. Results and Discussion

A. Plant Operating Conditions and Discharge Characteristics

Three experiments were conducted over two operational days between 17 October 2013 – 22 October 2013 to examine the brine discharge dynamics corresponding to plant operating configurations of 66% and 100% production. To satisfy the design Froude number criterion ($F > 20$) during 'hot standby' operation (i.e. production rates of <100%), the GCDP augments brine discharge with bypass seawater, which is thoroughly mixed with effluent at the plant prior to discharge. This augmentation process requires pumping of extraneous seawater, and thus, incurs an additional operating cost to ensure the diffuser performs as designed.

There is an approximate 2-hour effluent migration period from the GCDP outfall shaft to the offshore brine diffuser [12] and the presented field experiment data accounts for this lag. Salinity measurements are expressed in terms of absolute salinity (S_A) and are derived using the TEOS-10 equations [13]. Outfall salinity (S_{A_0}) was determined from measurements at the GCDP outfall shaft. Ambient salinity (S_{A_a}) is determined from CT sensors located in the coastal ocean along the distant edge of the monitoring array - approximately 60 m to the SE of the examined diffuser port at 12.5 m elevation above the seafloor. Evidence from modelling and field data indicate associated salinity variability at this location is dictated by background oceanic processes and the effects of SWRO discharge are negligible.

Mean background and effluent characteristics are presented in Table I. Herein, experimental regimes are designated with a respective case number. Assuming even distribution of total volumetric flux (Q_T) across the diffuser, mean outflows at the nominal diffuser port $\overline{Q_0}$ ranged 0.129 – 0.159 $m^3 \cdot s^{-1}$. Jet-densimetric Froude numbers (F) ranged 17.66 – 29.83 across all experiments. For approximately 17–19 hours prior to the commencement of the first case for each experiment day, the GCDP operated in seawater bypass mode.

B. Ambient Characterization

1) Ambient Crossflow

Coastal processes at the GCDP offshore brine diffuser are inherently complex and drive considerable transient and spatial variability over the full depth of the water column. Ambient crossflow properties are shown in Fig. 3. The measured water depth was 18.43 ± 0.50 m and tidal variations show a combination of M_1 and M_2 mechanisms; however, their relative influence on measured crossflow was negligible. Velocity magnitude is consistently higher ($U_a \approx 0.5$ $m \cdot s^{-1}$) in the upper 1.0 m of the water column, with flows attributed to wind-forcing. Below this region, ambient crossflow varies considerably across each case regime in response to various longshore mechanisms, with horizontal velocities ranging 0.0 – 0.4 $m \cdot s^{-1}$. Vertical velocity was determined to be negligible across all examined cases ($U_{a_w} < 0.01$ $m \cdot s^{-1}$).

Quantifying the effects of ambient velocity magnitude on discharge response, the crossflow-based Froude number (u_rF) was derived over the depth of the water column from the mean effluent density and real-time ambient density (determined from background sensors situated 60 m from the diffuser at 12.5 m elevation). Case 1-1 (17 October 2013) presents a SSE surface-driven mobilization event, exhibiting a general trend of increasing influence over the depth of the water column and increasing velocity magnitude, with $u_rF > 1$ above 5 m elevation in the second half of the case duration.

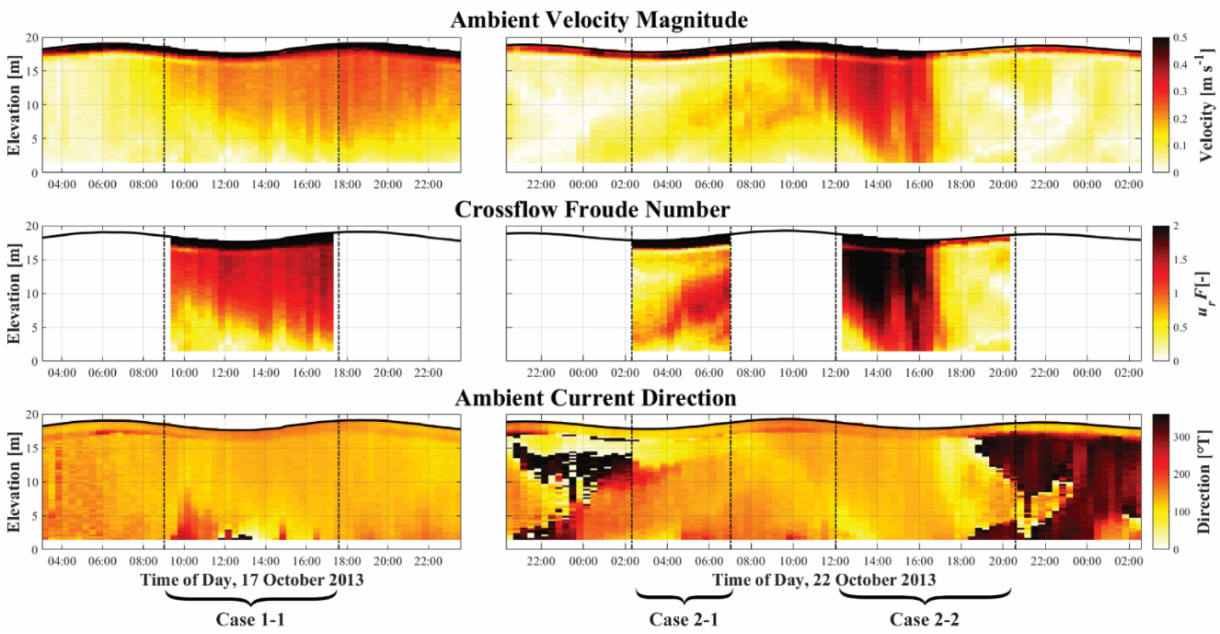

Fig. 3 ADCP profiles of horizontal current magnitude, ambient crossflow Froude number and direction. Direction uses the convention of true bearing and refers to the direction of propagation. Solid black line presents change of water depth due to tides

TABLE I
EXPERIMENT DISCHARGE PROPERTIES

Case Number	Quantity	Start Date at GCDP	End Date at GCDP	$\overline{Q_0}$ [m^3·s^{-1}]	$\overline{S_{A_0}}$ [g·kg^{-1}]	$\overline{S_{A_a}}$ [g·kg^{-1}]	$\overline{\rho_0}$ [kg·m^3]	$\overline{\rho_a}$ [kg·m^3]	F [-]
1-1	100%	Oct. 17, 07:01	Oct. 17, 15:35	2.23	53.49	39.87	1038.19	1028.11	23.63
2-1	66%	Oct. 22, 00:19	Oct. 22, 05:01	2.07	45.99	38.85	1032.60	1027.14	29.83
2-2	66% - minimal dilution	Oct. 22, 10:02	Oct. 22, 18:35	1.81	54.59	38.96	1039.18	1027.26	17.66

Experiment day two (22 October 2013) demonstrated mostly SE propagation in the lower 10 m of the water column. For Case 2-1, currents were dictated by flow mechanisms at approximately mid-depth, with increasing velocity trends over the case duration. Crossflow Froude numbers were considerable, with $u_rF \approx 1$ at 5 m elevation and notable mobilization of the lower regions of the water column over the full duration. Case 2-2 was subject to considerable hydrodynamic variability. The first half of the duration was influenced by a mobilization event over the depth of the water column with $u_rF \gg 1$. While ambient crossflow reduced considerably ($u_rF < 0.5$), the later stages of Case 2-2 were subject to velocity shear, with elevations 0 – 4 m and 10 – 17 m propagating NW, contrasting the SE flows of the remaining constituents of the water column.

2) Waves

Recorded wave properties are presented in Table II. Across all cases, mean significant wave height was observed to range from 1.2 – 1.4 m, while mean wave periods ranged 4.5 – 8.5 s. Waves were observed to propagate from the NNE – E, approximately perpendicular to discharge, with ϕ_w ranging -65° – -105° relative to the nominal discharge port.

Wave behaviors have been extrapolated using linear wave theory [14]. Transitional regimes ($H_a / L < 0.5$) were determined for experiment day two, while Case 1-1 was subject to a deep wave scenario. Maximum orbital particle velocities were determined at port elevation (U_{w,Max_0}). Provided the deep wave regime of Case 1-1 ($H_a / L > 0.50$), wave induced particle velocities at discharge elevation are considered negligible. Longer wave periods experienced on experiment day 2 yielded increased maximum orbital velocities at port elevation, with magnitudes approximately equating to 10% of discharge velocity (U_0 = 3.3 m·s^{-1} and 2.9 m·s^{-1} for Case 2-1 and 2-2, respectively). Albeit their temporal nature, horizontal wave-induced velocities for experiment day 2 are comparable to the measured ambient crossflow velocities – potentially influencing discharge response.

TABLE II
EXPERIMENT WAVE PROPERTIES

Case Number	H_w [m]	T [s]	H_a / L [-]	U_{W,MAX_0} [m·s^{-1}]	ϕ_w [°T]
1-1	1.2 ± 0.2	4.5 ± 0.2	0.56 ± 0.04	0.04 ± 0.01	42 ± 12
2-1	1.2 ± 0.1	8.5 ± 0.0	0.19 ± 0.00	0.30 ± 0.02	60 ± 12
2-2	1.4 ± 0.1	8.3 ± 1.5	0.24 ± 0.16	0.32 ± 0.11	59 ± 16

H_w and T denote wave height and wave period respectively. L denotes wavelength. U_{w,Max_0} presents maximum horizontal wave induced velocity at port elevation. ϕ_w denotes wave direction relative to direction of origin in degrees true.

C. Measured Salinity Change

Measured salinity changes were determined relative to a 1-hour ensemble average, commencing 3-hours prior to the anticipated first arrival of discharge of the first case corresponding to each experimental day. Beyond 17 October 2013, marine fouling of static instruments was observed. This was determined to be most pronounced on equipment situated near the seafloor – in particular, instruments situated at 0.5 m elevation. Fouled CT sensors (evident by data anomalies or sensor drift) were subsequently discarded from the proceeding analysis.

Mean salinity changes recorded at source elevation (2.5 m above the seafloor) are shown in Fig. 4. Applying quiescent-based empirical formulations presented in [4] (i.e. $Z_l = 0.7 \times dF$), the thickness of the spreading brine layer is determined to range 2.9 – 5.0 m. Thus, observations at 2.5 m elevation are contained within the brine density-induced sublayer. Salinity varied considerably, predominantly due to changes in background conditions. Relative to the Case 1-1 reference period, S_{A_a} ranged -0.80 – 2.67 g·kg^{-1} over the full experiment duration, with a mean salinity increase of 1.13 ± 0.74 g·kg^{-1}. The maximum observed ambient salinity occurred at approximately 23:00 h on 19 October 2013 – approximately 53 hours after the cessation of Case 1-1. Across all experiments, mean salinity changes ranged 0.11 – 0.83 g·kg^{-1} over the full 2.5 m elevation transect. Regulatory provisions require the GCDP diffuser to maintain salinity < 2 PSU (≈ 2 g·kg^{-1}) above background salinity at a distance 60 m from the diffuser. For each case this was consistently achieved, with mean salinity changes ranging 0.14 – 0.53 g·kg^{-1} at the edge of the monitoring array.

Case 1-1 presents 100% plant operation and subsequently yields a high rate of volumetric flux (Q_T = 2.23 m^3·s^{-1}) and a comparably high source salinity differential (i.e. ($\overline{S_{A_0}}$ – $\overline{S_{A_a}}$ = 13.62 g·kg^{-1}). Ambient crossflow directionality demonstrates relatively consistent co-propagating SE trends above 4 m. Below 4 m, directional components of mean flow vary, with weak ($u_rF \approx 0.1 – 0.5$) WSW and NE events recorded, prior to the full mobilization of the water column at approximately 14:00 h where SE trends dictate flow. Ambient salinity changes over Case 1-1 are low, with ΔS_{A_a} = -0.08 g·kg^{-1}. Salinity distributions (Fig. 4 (A)) appear to distinctly capture discharge behavior, with elevations in salinity recorded within 30 m of the diffuser. Central CT sensors along the horizontal transect exhibit relative increases in salinity – concurring with mean ambient flow directionality.

Ambient hydrodynamic properties play a considerable role for Case 2-1 and Case 2-2. Similar to Case 1-1, consistent SE propagation below 13 m elevation was observed over the Case 2-1 duration. Ambient mobilization at mid-depth dictated flow ($u_rF \approx 1.5$), with considerable effect on jet trajectory. Case 2-2 is governed by a surface-driven event, prior to the occurrence of complex bi-modal water-column shear at the experiment conclusion. Consistent with the considerable ambient crossflows observed and subjection to transitional wave regimes, spatial distribution of salinity changes were comparably minor, with variation at source elevation ranging 0.50 – 0.83 g·kg^{-1} and 0.40 – 0.72 g·kg^{-1} for Case 2-1 and Case 2-2, respectively.

D. Jet Properties

Jet trajectory characteristics and dilution at the near field have been determined and comparisons have been made against empirical scaling approaches set by [15] (Table III). Field trajectories were inferred from spatially interpolated salinity change distributions, where semi-quantitative analysis of transient variations and mean salinity changes were collectively examined.

1) Return Distance

With the appreciable decay of jet-imposed horizontal momentum at the end of the jets' trajectory for $\theta_0 = 60°$, the extent of horizontal jet translation at the seafloor (X_i) approximately equates to the return distance (X_r) (Fig. 1). Return distances (obtained from the 2.5 m elevation transect) have been extrapolated from field data. The horizontal trajectory extent was observed to vary appreciably over time (± 10 m) due to the variability of the ambient hydrodynamic conditions at the site and also due to the spatial distribution of the CT sensor arrays. Consistent with past studies concerning inclined jets subject to ambient crossflow (e.g. [7], [16]), each case subject to co-propagating currents demonstrated elongation in the horizontal direction, respective of quiescent-based empirical estimates. Similar trajectory ranges were observed for hot-standby regimes (Case 2-1 and Case 2-2). This comes despite their relative discrepancies in buoyancy and volumetric flux, which differ due to their respective complementing seawater bypass conditions. Given the comparable crossflow Froude numbers observed across equivalent case regimes, this suggests that ambient currents play a considerable role on jet behavior.

TABLE III
EMPIRICAL ESTIMATES AND EXPERIMENTAL OUTCOMES

Case Number	Computed Empirical Values [a]			Field Values	
	X_i [m]	X_n [m]	S_n [-]	X_r [m]	$\overline{S_{60}}$ [-]
1-1	15.47	53.43	61.44	10-20	62.55
2-1	19.52	67.45	77.56	20-30	15.75
2-2	11.56	39.93	45.92	10-30	67.89

[a]Computed values determined in accordance to empirical formulae presented in [15].

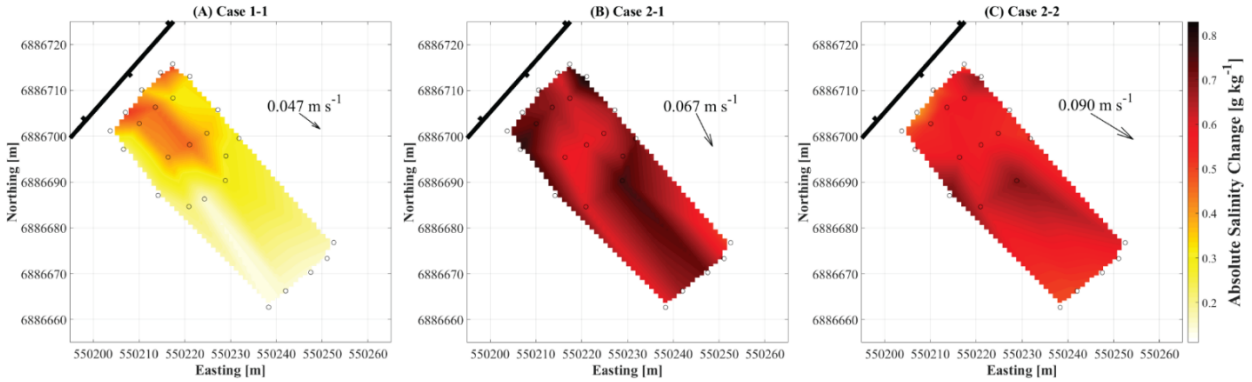

Fig. 4 Mean change in absolute salinity over experiment durations at 2.5 m elevation above seafloor. Mean current velocity vector coinciding with 2.5 m elevation also presented. Spatial linear interpolation is used between measured sensor locations (open black circle symbols)

2) Boundary Dilution

Mean dilution at the edge of the monitoring array has been determined in accordance with measured salinity change (Table III). The respective distance of 60 m from the diffuser is approximately consistent with the length of the mixing zone (X_n) under design conditions (determined by $X_n = 9.5 \times dF$ [15]) (Table III). Subsequently, the mean corresponding dilution ($\overline{S_{60}}$) and ultimate minimum dilution (S_n) are assumed to be comparable. $\overline{S_{60}}$ has been determined using (2):

$$\overline{S_{60}} = \frac{\overline{S_{A_0}} - \overline{S_{A_a}}}{\Delta\overline{S_{A_n}} - \Delta\overline{S_{A_a}}} \quad (2)$$

where $\overline{S_{A_n}}$ is the mean absolute salinity recorded at the far edge of the monitoring array at 2.5 m elevation. For Case 1-1, $\overline{S_{60}}$ dilution values yield high correlation with empirical quiescent estimates from [15]. Provided the low ambient salinity variability over this measured duration ($\overline{\Delta S_{A_a}}$ = -0.08 ± 0.05 g·kg^{-1}), it appears this outcome provides affirmation of the empirical methodology. Conversely, data from Case 2-1 and Case 2-2 showed considerable discrepancy between empirical estimates and derived field values. Ambient salinity variability for these cases were notably higher than Case 1-1 ($\overline{\Delta S_{A_a}}$ = 0.18 ± 0.09 g·kg^{-1} and $\overline{\Delta S_{A_a}}$ = 0.30 ± 0.51 g·kg^{-1} for Case 2-1 and Case 2-2, respectively), and hence, caution is advised when assessing their respective dilutions.

V. Conclusion

A field experiment was conducted to examine near field behavior of a submerged hypersaline discharge arising from an inclined multiport diffuser in a shallow, open-coastal embayment. Diffuser performance was considered for plant operations ranging 66 – 100%. The static CT monitoring system successfully captured signals arising from the SWRO outfall. Both hot-standby and 100% capacity plant operating regimes were identified to comply with the regulatory condition of < 2 g·kg^{-1} at a distance 60 m from the diffuser with a maximum recorded increase of 0.53 g·kg^{-1} at the edge of the monitoring array. Observed background salinity variability was determined to exceed salinity increases attributed to SWRO plant discharges over the experiment duration, ranging -0.80 – 2.67 g·kg^{-1}. The use of a tracer is subsequently advised for future field investigations to facilitate clearer spatial understanding of discharge behavior in the field.

While dense jet behavior in idealistic quiescent receiving environments is extensively documented in literature and widely adopted in field-scale industrial design processes, ambient processes captured in this study strongly contradict their design criterion. Crossflow and wave mechanisms dictated jet response, whereby detected horizontal trajectory components exceeded empirical estimates determined by [15]. In agreement with [7], changes in measured jet trajectory were most apparent when $u_rF > 0.5$ occurred below 5 m elevation. Future advances in the demonstrated understanding of dense discharges subject to turbulent crossflow processes, differing ambient velocity structures and wave processes are required to accommodate dynamic ambient interactions. Such progressions will facilitate an improved understanding of the performance of existing infrastructure and provide critical insight for future outfall designs.

Appendix

A. Linear Wave Theory

The extent of effect of a passing wave over the depth of the water column is dependent upon wavelength, L [L], and the mean ambient water depth, H_a [L]. These parameters are typically combined with the ratio H_a / L [-]. Generally, wave-induced seabed orbital particle velocities reduce with increasing H_a / L and are effectively nullified for deep wave regimes defined by $H_a / L > 0.50$. Ocean outfalls are typically located in the transitional or deep water regions, where $H_a / L > 0.05$. Applying linear wave theory, for transitional regimes the maximum horizontal particle velocity at a distance h [L]

from the mean water surface is determined by (3):

$$U_{w,Max} = \frac{H_w}{2}\frac{gk}{\omega}\frac{\cosh[k(h+H_a)]}{\cosh(kH_a)} \quad (3)$$

where T [T] is the wave period, $k = 2\pi / L$ [L^{-1}] is the wave number and $\omega = 2\pi / T$ [T^{-1}] is the angular frequency. In this paper, maximum wave induced velocity at port elevation is presented as U_{w,Max_0} [L T^{-1}], where $h = H_a - H_0$.

B. Notation and Dimensions

d	Port diameter [L]
F	Jet densimetric Froude number [-] defined as: $F = \frac{U_0}{\sqrt{g_0' d}}$
g	Acceleration due to gravity [L T^{-2}]
g_0'	Modified acceleration due to gravity [L T^{-2}] defined as: $g_0' = \frac{\rho_0 - \rho_a}{\rho_a} \times g$
h	Distance relative to mean water surface [L]
k	Wave number [L^{-1}] defined as: $k = \frac{2\pi}{L}$
H_0	Discharge port elevation [L]
H_a	Ambient depth [L]
H_w	Wave height [L]
L	Wavelength [L]
Q_0	Source volumetric flow rate [L^3 T^{-1}]
Q_T	Total diffuser volumetric flow rate [L^3 T^{-1}]
S	Jet dilution parameter [-]
S_{60}	Field dilution measured 60 m from the diffuser [-]
S_A	Salinity in ambient salinity units [M M^{-1}]
S_{A_0}	Effluent absolute salinity [M M^{-1}]
S_{A_a}	Ambient absolute salinity [M M^{-1}]
T	Wave period [T]
u_r	Ambient crossflow and jet exit velocity ration [-] defined as: $u_r = \frac{U_a}{U_0}$
u_rF	Crossflow-based Froude number [-]
U_0	Jet exit velocity [L T^{-1}]
U_a	Ambient velocity [L T^{-1}]
U_{a_w}	Vertical component of ambient velocity [L T^{-1}]
U_{w,Max_0}	Maximum wave-induced velocity at source elevation [L T^{-1}]
X_i	Horizontal trajectory distance to jet impact on lower boundary [L]
X_n	Horizontal distance to location of ultimate minimum dilution [L]
X_r	Horizontal trajectory distance to return elevation [L]
Z_l	Bottom layer thickness [L]
Z_t	Terminal rise elevation [L]
θ_0	Port inclination above horizontal [-]
ρ_0	Source discharge density [M L^{-3}]
ρ_a	Ambient density [M L^{-3}]
ϕ_a	Angle of ambient current propagation relative to discharge propagation [-] where $\phi_a = 0°$ denotes counter-propagating scenario
ϕ_w	Angle of wave propagation relative to discharge propagation [-] where $\phi_w = 0°$ denotes counter-propagating scenario
χ	Geometric jet parameter [L]
ω	Wave angular frequency [T^{-1}] defined as: $\omega = \frac{2\pi}{T}$

ACKNOWLEDGMENT

The authors acknowledge the financial support of the National Centre of Excellence in Desalination Australia, which is funded by the Australia Government through the Water for the Future Initiative.

REFERENCES

[1] L. O. Villacorte, S.A.A Tabatabai, N. Dhakal, G. Amy, J. C. Schippers, M. D. Kennedy, "Algal blooms: an emerging threat to seawater reverse osmosis desalination," Desalination and Water Treatment, vol. 55, pp. 2601 – 2611, 2015.

[2] S. Lattemann, and T. Höpner, "Environmental impact and impact assessment of seawater desalination," Desalination, vol. 220, no. (1–3), pp. 1-15, 2008.

[3] M. A. Zeitoun, W. F. Mcilhenny, and R. O. Reid, "Conceptual designs of outfall systems for desalting plants. Research and development progress (report no. 550)," United States Department of the Interior, 1st ed., 1970.

[4] P. J. W. Roberts, A. Ferrier and G. Daviero, "Mixing in inclined dense jets," Journal of Hydraulic Engineering, vol. 123, pp. 693 – 699, 1997.

[5] C. C. K. Lai, J. H. W. Lee, "Initial mixing of inclined dense jet in perpendicular crossflow," Environmental Fluid Mechanics, vol. 14, no. 1, pp. 25 – 49, 2014.

[6] A. B. Pincince and E. J. List, "Disposal of brine into an estuary," Journal (Water Pollution Control Federation), vol. 45, pp. 2335 – 2344, 1973.

[7] P. J. W. Roberts, and G. Toms, "Inclined dense jets in flowing current," Journal of Hydraulic Engineering, vol. 113, pp. 323 – 340, 1987.

[8] P. J. W. Roberts, "Near field flow dynamics of concentrate discharges and diffuser design," in Intakes and Outfalls for Seawater Reverse-Osmosis Desalination Facilities, T. M. Missimer, B. Jones, R. G. Maliver, Switzerland: Springer International Publishing, 2015, pp. 369 – 396.

[9] P. Baudish, "Design Considerations for Tunnelled Seawater Intakes," in Intakes and Outfalls for Seawater Reverse-Osmosis Desalination Facilities, T. M. Missimer, B. Jones, R. G. Maliver, Switzerland: Springer International Publishing, 2015, pp. 19 – 38.

[10] O. Abessi, and P. J. W. Roberts, "Multiport diffusers for dense discharges," Journal of Hydraulic Engineering, vol. 140, pp. 04014032, 2014.

[11] Geoscience Australia (2017). "Australian Geomagnetic Reference Field Values, for latitude: -28.1325°, longitude: 153.5117°, date: 20 October 2013", Online calculator, http://www.ga.gov.au/oracle/geomag/agrfform.jsp, accessed 23 January 2017.

[12] B. Gibbes, A. Grinham, S. Albert, P. Fisher, M. J. Baum, and D. Gale, "Measurement of receiving environment conditions at a salt water reverse osmosis seafloor brine diffuser: experimental observations from the Gold Coast Desalination Plant," Queensland, Australia: The University of Queensland, 2016.

[13] T. J. McDougall and P. M. Barker, "Getting started with TEOS-10 and the Gibbs seawater (GSW) oceanographic toolbox," SCOR/IAPSO WG127, pp. 28, 2011.

[14] R. G. Dean, R. A. Dalrymple, Water wave mechanics for engineers and scientists, Advanced Series on Ocean Engineering, vol. 2, Singapore: World Scientific, 1991, pp. 78 – 86.

[15] O. Abessi, and P. J. W. Roberts, "Dense jet discharges in shallow water," Journal of Hydraulic Engineering, vol. 142, pp. 04015033, 2015.

[16] P. J. W. Roberts, and O. Abessi, "Optimization of desalination diffusers using three-dimensional laser-induced fluorescence," Report Prepared for United States Bureau of Reclamation Agreement Number R11 AC81 535, School of Civil and Environmental Engineering, Georgia Institute of Technology, Atlanta, GA, 2014.